Pak. j. sci. ind. res. Ser. A: phys. sci. 2025 **68A**(2) 125-134

Adsorption of Aqueous Phosphate by Thermally Aged MgFe Layered Double Hydroxides: Kinetics and Characterizations

Atin Nuryadin[a]* and Tsuyoshi Imai[b]
[a]Department of Physics Education, Mulawarman University, Jl. Muara Pahu Gunung Kelua Campus,
Samarinda, Kalimantan Timur-75123, Indonesia
[b]Graduate School of Sciences and Technology for Innovation, Yamaguchi University,
Tokiwadai 2-16-1, Ube, Yamaguchi-755-8611, Japan

(received February 28, 2024; revised August 6, 2024; accepted August 7, 2024)

Abstract. In layered double hydroxides (LDH) synthesis, calcination increasingly attracts attention because it increases adsorption capacity. Despite this, since the calcination process caused the layers of LDH to be disordered, the thermal treatment process used to improve LDH crystallinity before calcination seems unnecessary. This study elucidates the effect of thermal aging on the phosphate adsorption ability of MgFe-LDH which was previously unexplained. Uncalcined and calcined MgFe-LDH adsorbents with different Mg/Fe molar ratios (2-4) were prepared by co-precipitation. Thermally aged and calcined MgFe-LDH with an Mg/Fe ratio of 3 showed the most effective adsorption. The pseudo-second-order model provided the best description of the kinetic adsorption data. XRD analysis showed that thermal aging improves the crystallinity of MgFe-LDH before calcination, which results in high adsorption of LDH after calcination because it leads to better reconstruction possibility. This study provides additional insight into the preparation of the Mg-Fe-LDH for water phosphate removal.

Keywords: adsorption kinetics, layered double hydroxides, phosphate adsorption, thermal aging

Introduction

Adsorption is a situation where atoms, ions, or molecules from a gas, liquid or dissolved solid adhere to the surface of another substance, forming a film of the adsorbate on the adsorbent (Osali *et al*., 2023). Unlike absorption which penetrates the bulk of a material, this process is driven by surface forces. Adsorption can be categorized into physiosorption, driven by weak van der Waals interactions and chemisorption, characterized by covalent or ionic bonding (Raji *et al*., 2023). Adsorption plays a vital role in a range of natural, physical, biological, chemical systems and is widely utilized in industries for applications such as air purification, water treatment and catalysis (Rápó and Tonk, 2021; Qu, 2008). Specifically, in environmental science, adsorption is an important process for extracting phosphate ions from water bodies to prevent eutrophication and preserve ecological balance (Sun *et al*., 2013).

Phosphorus is one of the fundamental nutrients to sustain daily life, affecting every organism on earth (Tang *et al*., 2020). However, its accumulation along with nitrogen, is the main factor of eutrophication in surface waters which causes algal bloom and deteriorates water quality (Ding *et al*., 2020). Therefore, removing phosphorus from domestic wastewater before discharge is essential to reduce the risk of eutrophication in natural waters. It has become obligatory and common in many countries, leading to the exploration of alternative wastewater treatment technologies for phosphorus removal. In wastewater treatment the adsorption is an attractive alternative due to its simplicity, low cost and superior effectiveness (Bacelo *et al*., 2020).

Layered double hydroxide (LDH) materials suggested to be potential phosphate adsorbents because of their ability to remove phosphate from a solution by interlayer anion exchange and surface adsorption (Goh *et al*., 2008). LDH materials naturally show excellent adsorption toward various anions, including phosphate and due to their positively charged layers and weak interlayer binding (Peng *et al*., 2014). This excellent adsorption property has led to a study of various LDHs to adsorb phosphate from water, such as MgAl-LDH, ZnAl-LDH, MgMn-LDH and MgFe-LDH (Nuryadin and Imai, 2021a; Lai *et al*., 2020; Iftekhar *et al*., 2018; Novillo *et al*., 2014). The calcination process in LDH synthesis is increasingly attracting attention because it can enhance the adsorption capacity because of the rehydration and structure re-construction phenomenon in LDH (Sun *et al*., 2013).

---

*Author for correspondence;
E-mail: atinnuryadin@hotmail.com

A proper method for the adsorbent preparation is crucial to improve adsorption ability, it is not easy to considering the control of their structures accurately. The phosphate adsorption property of the same material could vary depending on the preparation method (Miyauchi *et al.*, 2009). Generally, the synthesis of LDH materials uses a simple and commonly used co-precipitation method at high supersaturation (Goh *et al.*, 2008). A thermal aging process usually follows this method to ensure the yields and crystallinity of the LDH materials (Hussein *et al.*, 2001). However, LDHs calcined at elevated temperature had broad X-ray diffraction (XRD) peaks, indicating a poor long-range ordered phase of nanocrystalline material with exceedingly small nanoparticles or even an amorphous phase (Das *et al.*, 2007). According to XRD patterns, the calcination process caused the structure of the material to become disordered. Considering this, it seems that thermal treatment is not necessary for the preparation of calcined LDHs for phosphate adsorbent.

In this study, uncalcined and calcined MgFe-LDH was synthesized for phosphate adsorbents. The effect of heat aging during synthesis on the phosphate adsorption ability of the adsorbents was carefully investigated. The study of MgFe-LDH as a phosphate adsorbent has been done by some earlier researchers (Kim *et al.*, 2020; Sun *et al.*, 2013; Du *et al.*, 2009). However, the best of the author's knowledge, the investigation of the thermal aging effect on the phosphate adsorption ability of calcined LDH has not been conducted. Moreover, adsorption kinetics models were applied to explain phosphate adsorption properties by thermal aged MgFe-LDH. The characteristics of the synthesized MgFe-LDH were investigated by means of X-ray diffraction (XRD), Fourier transform infrared (FTIR) and scanning electron microscopy/energy dispersive X-ray spectroscopy (SEM/EDX) analyses.

It is crucial to characterize and analyze the kinetic processes in this research for some reasons. Characterization helps identify the structural and surface properties of materials used for phosphate removal, which is vital for understanding how these materials interact with phosphate ions at a molecular level. Kinetic studies provide insights into the rate of phosphate adsorption, essential for designing efficient and effective removal systems. Knowing kinetics allows for the optimization of contact time and material usage, ensuring maximum phosphate uptake. Understanding materials and their kinetic behaviour allows us to predict their performance in real-world applications, thereby reducing the environmental impact of agricultural phosphate overuse. Phosphate management solutions based on characterization and kinetics balance agricultural benefits with environmental protection.

Materials and Methods

This study used analytical pure-grade reagents supplied by Fujifilm wako pure chemical corporation, including $FeCl_3 \cdot 6H_2O$, $MgCl_2 \cdot 6H_2O$, Na_2CO_3, K_2HPO_4, NaOH and HCl. These chemicals were used without further purification. Metal salt solutions were prepared using deionized (DI) water.

Preparation of MgFe-LDH. The MgFe-LDH materials were synthesized by the co-precipitation method. The 10 mL of 1 M $FeCl_3$ solution was mixed with 20, 30 and 40 mL of 1 M $MgCl_2$ solution to obtain Mg-Fe LDH with different ratios of Mg to Fe (2:1, 3:1 and 4:1). This mixed solution of $MgCl_2$ and $FeCl_2$ was added dropwise to 200 mL of deionized water under vigorous stirring. Simultaneously, the second mixture of 1 M NaOH and 1 M Na_2CO_3 solutions with a 3:1 volume ratio was added to the beaker and stirred for 30 min. The pH of about 10 was maintained using NaOH and NaCl solutions. As for comparison, the separated suspensions of the previous process were thermally aged for 24 h at 80 °C in an oven and room temperature, respectively, to obtain thermal and room temperature aged LDHs. In the aging process, molecules or ions are given sufficient time to arrange themselves into ordered structures, to promote nucleation, the initial formation of crystals (Nguyen *et al.*, 2023). The resulted precipitates after aging were filtered and washed with deionized water until pH was about 7 and subsequently dried at 80 °C for 24 h. The samples were dried to remove excessive water content. Calcined samples were obtained by heating at 573 K for 3 h to get two different types of LDHs, uncalcined and calcined samples.

Batch adsorption experiments. Batch adsorption experiments were performed using synthetic phosphate solution stock. This stock was prepared using NaH_2PO_4 (99.0%) diluted by DI water to intended concentrations. The solution pH was adjusted to 6 using diluted HCl and NaOH. The adsorbent (0.02 g) was added to 100 mL of the phosphate solution (30 mg/L) and shaken at a speed of 140 rpm at about 30 °C for 24 h. The supernatant was filtered using a 0.45 μm filter for phosphate concentration analysis. The remaining phosphate concentration was analyzed using the molybdenum blue method (Japanese Industrial Standards-JIS K102.46.3-2000) and a Hitachi U-1800 UV/vis spectrophotometer at a wavelength of 880 nm. The phosphate adsorption capacity q_e (mg/g) was determined using equation (1):

$$q_e = \frac{C_0 - C}{m} \times V \quad \text{.......................................} \quad (1)$$

where:

C_0 and C are the initial and residual phosphate concentrations (mg/L), respectively, V is the volume of the solution (L) and m is the mass of the adsorbent (g). The adsorption kinetics study was conducted by shaking a 0.02 g sample in 100 mL of 30 mg/L phosphate solution. Phosphate concentrations were determined from supernatants at intervals ranging from 1 h to 96 h.

Characterization of MgFe-LDH. The XRD spectra of MgFe-LDH were recorded on a Rigaku Ultima IV protectus diffractometer for the crystallinity analysis using Cu-Kα radiation at 40 kV at a scanning rate of 1°/min in the 2θ angle range from 5° to 70°. The micrographs and EDX data of the samples were obtained using scanning electron microscopy (SEM) images were collected by using a JEOL JSM-7600F field emission SEM at an accelerating voltage of 5 kV at magnifications of 5000 and 10000. Fourier-transform infrared (FTIR) spectra analysis was achieved by a Jasco FT/IR-4600 spectrophotometer in the region of 4000-600/cm.

Results and Discussion

Phosphate adsorption. The effect of thermal aging and calcination on the phosphate adsorption ability of MgFe-LDH with different ratios of Mg to Fe as shown in Fig. 1. Where R and T represent room temperature and thermally aged LDH and U and C represent uncalcined and calcined LDH, respectively. The phosphate adsorption of uncalcined LDH samples shows an increase in adsorption capacity with an increase in the ratio of Mg:Fe from 2 to 4 for both thermal and room temperature aged samples. Nonetheless, calcined MgFe-LDH samples tend to have more significant adsorption than their uncalcined counterparts, especially for thermally aged samples. The surface adsorption and memory effect (layered structure reconstruction) were responsible for phosphate adsorption in the calcined MgFe-LDH, while only anion exchange primarily controlled phosphate adsorption in the uncalcined MgFe-LDH (Ferreira *et al.*, 2004).

Uncalcined MgFe-LDHs showed an elevated adsorption capacity as the Mg to Fe ratio increased. On the other hand, the calcined MgFe-LDH with an Mg to Fe ratio of 3 represents the maximum adsorption capacity. This result agrees with the study reported by previous studies (Kamimoto *et al.*, 2019; Abdelkader *et al.*, 2011). It could be speculated that the introduction of Mg^{2+} to Mg:Fe ratio of 3 initially improves the layered structure of the MgFe-LDH and increases the phosphate adsorption (Sun *et al.*, 2013). However, further intercalation of Mg^{2+} produces MgFe-LDHs with a lower amount of Fe^{3+}, reducing the net positive charge on the hydroxide layer (Das *et al.*, 2006). Based on this result, the calcined MgFe-LDH sample with thermal aging and an Mg:Fe ratio of 3 was chosen for the following adsorption study and the term 'MgFe-LDH' is used hereafter to refer to this sample.

Adsorption kinetics. Adsorption kinetics is the most vital parameter to examine when designing an adsorption system because it influences the applicability and cost of the adsorption process. Adsorption kinetics of phosphate was studied at room temperature using the constant initial phosphate concentrations of 30 mg/L with a 96 h contact time. The adsorption rate of RC and TC samples is depicted in Fig. 2. The adsorption in both samples started with rapid adsorption for about 13 h, followed by slow adsorption until reaching

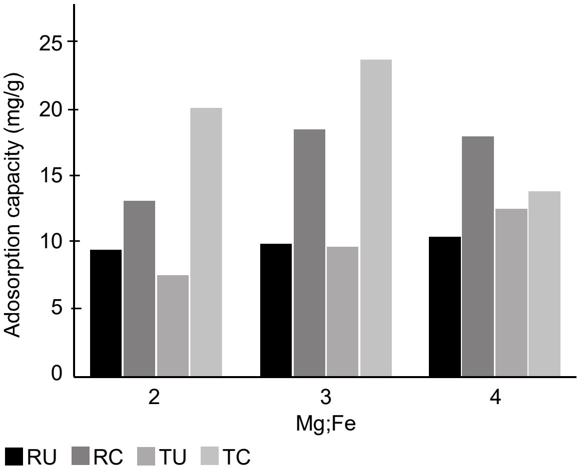

Fig. 1. Phosphate adsorption capacity of MgFe-LDHs with different synthesis conditions (C_0 = 30 mg/L; m = 0.03 g; V = 100 mL; T = ~303 K; pH = 6; t = 24 h).

equilibrium. The initial rapid adsorption can be attributed to the abundant availability of vacant adsorption sites on both the surface and interlayer of MgFe-LDH. These sites were nearly saturated after 24 h of contact time, achieving approximately 95.52% and 98.58% adsorption for RC and TC samples, respectively, assuming near completion by 96 h. Despite reaching equilibrium around the same time for both RC and TC, RC exhibited a significantly lower adsorption capacity compared to TC. This discrepancy suggests variations in surface characteristics or interlayer structures of both samples that influence the kinetics of phosphate adsorption.

The experimental results were fitted to the three typical kinetic models frequently used to simulate the adsorbent-adsorbate interaction: pseudo-first-order, pseudo-second-order and Elovich. Pseudo-first-order assumes that adsorption occurs *via* diffusion through the adsorbent surface. In contrast, the pseudo-second-order kinetic model assumes the adsorption process is controlled by adsorption reaction at the adsorbent surface. The linear forms of pseudo-first-order and pseudo-second-order are expressed as equations 2 and 3 (Liu and Zhang, 2015).

$$\ln(q_e - q_t) = \ln(q_e) - k_1 t \quad \text{...} \quad (2)$$

$$\frac{t}{q_t} = \frac{1}{k_2 q_e^2} + \frac{1}{q_e} t \quad \text{..} \quad (3)$$

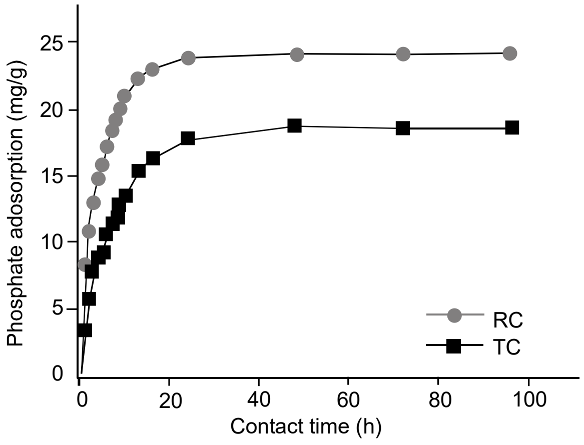

Fig. 2. Adsorption kinetics data for phosphate onto the calcined MgFe-LDHs synthesized by room temperature aging (RC) and thermal aging (TC) (C_0 = 30 mg/L; m = 0.03 g; V = 100 mL; T = 303±1). K; pH = 6).

where:

q_e and q_t (mg/g) are the amount of adsorbed phosphate at equilibrium and time t, respectively; k_1 (1/h) and k_2 (g/mg.h) are the rate constant of the pseudo-first-order model and pseudo-second-order model, respectively. The Elovich model assumes that the adsorption rate exponentially decreases as the amount of adsorbed solute increases on the adsorbent surface without any interaction among adsorbed species. This model is represented as equation 4 (Akinpelu *et al.*, 2021).

$$q_t = \frac{\ln(a_e b_e)}{b_e} + \frac{1}{b_e} \ln t \quad \text{....................................} \quad (4)$$

where:

a_e is the initial adsorption rate (mg/g.h) and b_e is related to the extent of surface coverage and activation energy for chemisorption (mg/g).

The linearity plots of pseudo-first-order, pseudo-second-order and Elovich are illustrated in Fig. 3. The detailed parametric values are shown in Table 1 which is based on the R^2 values and proven that the pseudo-second-order was the most suitable model for describing the kinetics of phosphate adsorption on the LDH. Moreover, the calculated adsorption capacity of q_e (24.27 mg/g) from pseudo-second-order was closer to the experimental value q_e (23.67 mg/g) than pseudo-first-order and Elovich model. This suggests that the phosphate adsorption process onto MgFe-LDH mainly occurred through chemical interaction.

Table 1. Kinetic model parameters for phosphate adsorption onto LDH

Kinetics model	Parameter	Value
Pseudo-first-order	q_c (mg/g)	19.01
	k_1 (1/h)	0.1727
	R^2	0.9952
Pseudo-second-order	q_c (mg/g)	24.27
	k^2 (g/mg·h)	0.0209
	R^2	0.9992
Elovich	q_c (mg/g)	26.79
	a_e (mg/g·h)	57.75
	b_e (mg/g)	0.2734
	R^2	0.8731

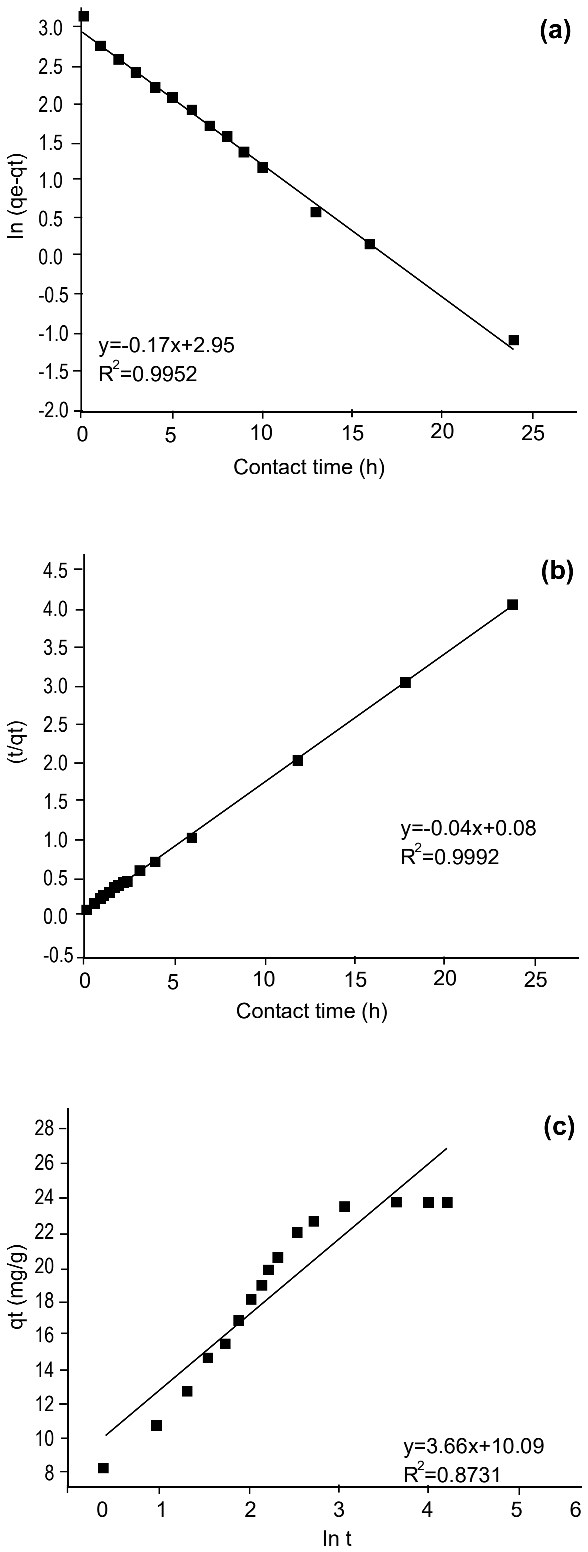

Fig. 3. Kinetic modeling linear plot for phosphate adsorption ions by LDH, **(a)** pseudo-first-order, **(b)** pseudo-second-order and **(c)** Elovich models.

In order to interpret the diffusion mechanism, the intra-particle diffusion model was applied. The parameter of this model can be determined Weber-Morris equation expressed by equation 4 (Weber and Morris, 1963).

$$q_t = k_{di}t^{1/2} + C$$

where:

k_{di} is the intra-particle diffusion rate constant (mg/g·$h^{1/2}$), and C is a constant calculated from the slope and intercept of the linear plot. If the plot of q_t *vs* $t^{1/2}$ is a linear plot over the time range, the intra-particle diffusion is a rate-limiting step (Pholosi *et al.*, 2020). The plot in Fig. 4, adsorption amount of phosphorus and the square root of time according to the time-resolved uptake curves of phosphorus in LDH and the values of intra-particle diffusion model parameters are shown in Table 2. Using the intra-particle diffusion model, if the plot passes through the origin, only intraparticle diffusion is the rate-limiting step, otherwise, boundary layer control would be involved (Liu *et al.*, 2010). In this study, the intra-particle diffusion plot was divided into two successive regions with different slope linear plots. This suggests that intra-particle diffusion was not the only rate-limiting step in the adsorption process but consisted of two processes. In the first process, phosphate adsorption was predominantly controlled by external surface diffusion from bulk to the most accessible active sites on the MgFe-LDH surface and interlayer through a boundary layer. The $k_{di,2}$ was smaller than $k_{di,1}$ suggested that the slope of the second stage is smaller

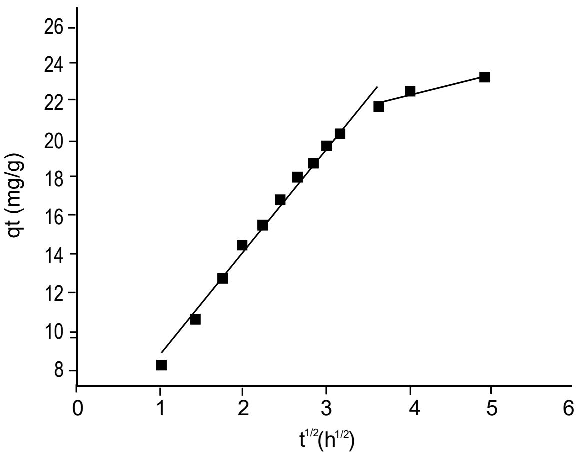

Fig. 4. Intra-particle diffusion plots for the adsorption of phosphate ions onto LDH.

than obtained for the first stage, thus the adsorption process was slower. The second process represented the slow pore diffusion process of phosphate ions from the adsorbent surface to the inner pores.

Characterization. The morphology of the MgFe-LDH surface was characterized by SEM and the SEM images are presented in Fig. 5(ab). The images show that the synthesized LDH has a porous and rough surface with crystal clusters on a nanometric scale. The structure was identified as platelet like layered shapes arranged together *via* face-to-face contact. The elemental analysis using the EDX spectrum, as depicted in Fig. 5(c), confirmed the presence of magnesium and iron in the synthesized LDH material walls. The chemical composition of the material obtained from EDX analysis as shown in Table 3. The molar ratio of Mg^{2+}/Fe^{3+} obtained from the EDX result clearly indicated that this result was in good agreement with the calculated molar ratio of about 3 used in the adsorbent preparation. The analysis also showed the presence of carbon, suggesting the existence of carbonate in the LDH interlayer.

The Cu-Kα powder XRD analysis was conducted on the synthesized LDH and the resulting patterns are presented in Fig. 6. The formation of LDH material after the co-precipitation process was confirmed by

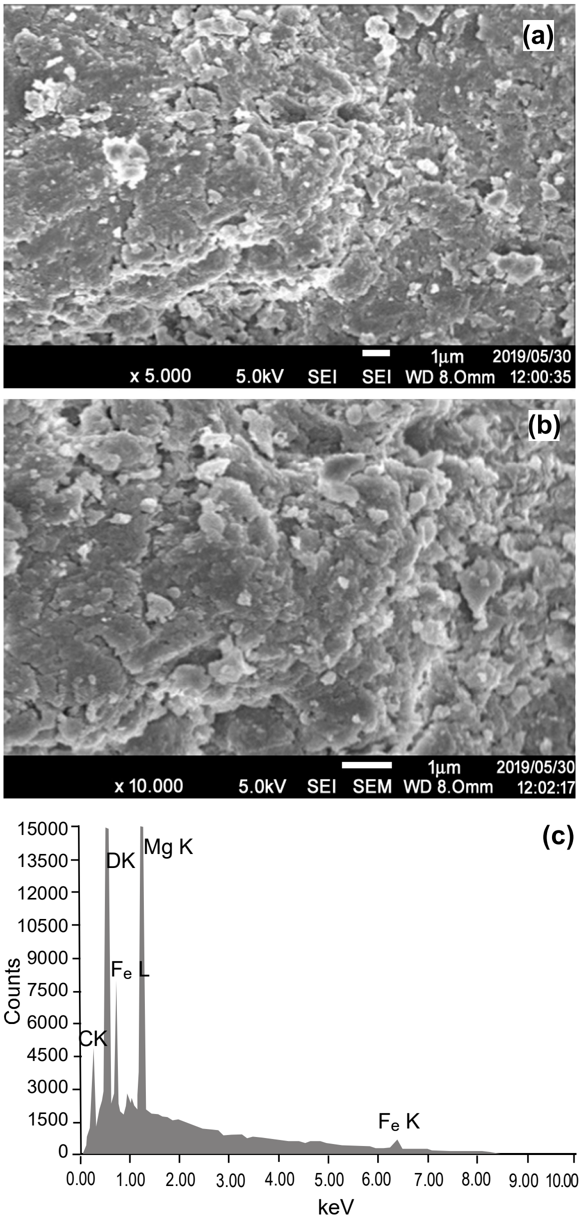

Fig. 5. SEM images at **(a)** 5000 times; **(b)** 10000 times magnification and **(c)** EDX analysis of LDH powder.

Table 2. Intra-particle diffusion model parameters for phosphate adsorption onto MgFe-LDH

Parameter	Value
k_{di1}	5.398
R_1^2	0.9900
k_{di2}	1.103
R_2^2	0.9807

Table 3. Chemical composition based on EDX analysis

Mg(wt.%)	Fe(wt.%)	O(wt. %)	C(wt. %)	Mg^{2+}/Fe^{3+}
26.72	8.21	57.75	7.33	3.25

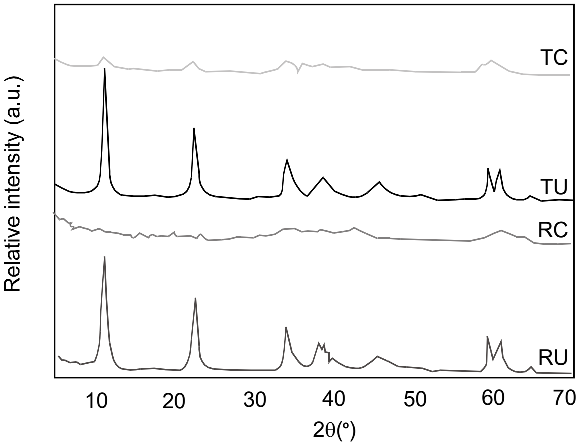

Fig. 6. X-ray powder diffraction patterns of MgFe-LDHs with different synthesis conditions.

powder XRD patterns. The diffraction peaks of uncalcined samples (RU and TU) showed a hexagonal lattice with rhombohedral 3R symmetry and indexed to (003), (006), (012), (015), (018), (110) and (113) planes of characteristic crystalline LDH materials (Nuryadin *et al.*, 2021; Cavani *et al.*, 1991). Significant changes were observed in the XRD patterns of MgFe-LDH after calcination. The sharp and well-defined peaks had mostly disappeared and replaced by broad peaks, suggesting that the layered structure of LDH was mainly decomposed due to the removal of water and carbonates from the interlayer.

For uncalcined MgFe-LDH which is observed a stronger XRD peak intensity on TU than RU and as indicated in Fig. 6. This result suggests that the hydrothermal method could facilitate the growth of MgFe-LDH crystals and increase crystal size. This is consistent with that previously reported by a previous study (Bhavani *et al.*, 2021). Therefore, MgFe-LDH synthesized by thermal aging should exhibit more ordered layer structures compared to those aged at room temperature. This suggests that the thermal aging process promotes better crystallinity and a more uniform arrangement of the layers within the MgFe-LDH structure.

Calculated LDH lattice parameters of RU and HU are compared in Table 4. In the case of RC and HC, lattice parameters could not be calculated due to the broad and low-intensity XRD peaks. The parameter *a* ($2d_{110}$) is the mean of the cation-cation distances within lamellar layers and c ($3/2[d_{003} + 2d_{006}]$) provides the total thickness of interlayer space and hydroxide sheet of brucite-like structure. Lattice parameter-a was almost identical between RU and TU, indicating that the average distance between two neighbouring cations in the LDH layer was not affected by thermal aging treatment. However, thermal aging slightly decreased the lattice parameters c. The strength of electrostatic attraction between interlayer anions and positively charged layers of LDH is one that determines the c value (Cosano *et al.*, 2020). Thus, the decrease in the c value of thermally aged LDH might be due to a stronger electrostatic interaction between the well-ordered positively charged hydroxide layers and the negatively charged interlayer anions as a result of a more crystalline form (Miyauchi *et al.*, 2009).

Table 4. Calculated lattice parameters of MgFe-LDH samples

Samples	Lattice parameters (nm)	
	a	*c*
RU	0.311	2.342
TU	0.310	2.333

The FTIR spectra of the MgFe-LDH, before and after the phosphate adsorption, are depicted in Fig. 7. The FTIR spectrum of as synthesized LDH was the typical spectra for LDH material, as composed of a strong and broad band centered at 3430/cm (OH stretching vibration of hydroxyl groups in the hydroxide sheets and water in the interlayer), a band at 1640/cm (structural O-H bending vibrations of physically adsorbed water) and an intense peak at 1358/cm (CO_3^{-2} antisymmetric stretching in the interlayer) (Novillo *et al.*, 2014). The band of CO_3^{-2} antisymmetric stretching was diminished after phosphate adsorption, suggesting that the number of carbonate anions in the LDH interlayer decreased as exchanged by phosphate anions during the adsorption process. The presence of new peaks at around 1095/cm and 989/cm (vibrational bands of P-O) after the adsorption experiment confirmed phosphate adsorption by the LDH (Ahmed *et al.*, 2019; Li *et al.*, 2016; Novillo *et al.*, 2014; Liu *et al.*, 2013). It stood for that the anion exchange played a significant role in phosphate adsorption on the calcined LDH.

The series of phosphate adsorption experiments revealed that thermally aged MgFe-LDH showed a higher adsorption capacity than that aged at room temperature.

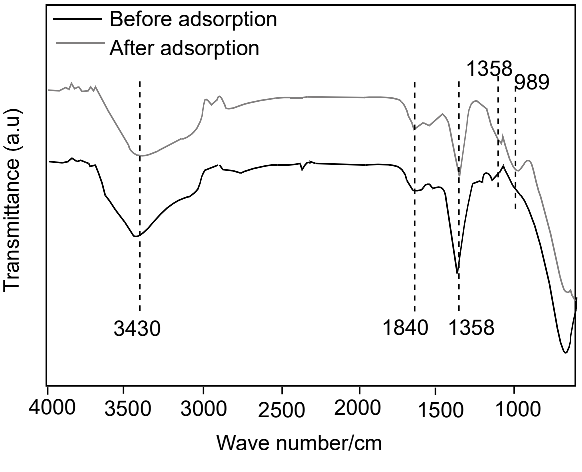

Fig. 7. FTIR spectra of the LDH before and after adsorption.

To explain this adsorption increase, the illustration of thermal aging contribution to the adsorption of phosphate onto LDH is proposed based on the XRD analysis, as illustrated in Fig. 8. Since the adsorption of phosphate anions on calcined LDH is significantly influenced by structural reconstruction. A more ordered structure in the original uncalcined MgFe-LDH facilitates greater removal of phosphate anions from aqueous solutions. Thermal aging enhances the crystallinity of MgFe-LDH, leading to increased adsorption capacity compared to room-aged samples.

In this study, the batch method was employed to assess the adsorption capacity of thermally aged calcined MgFe-LDH for phosphate removal. However, for practical applications in industries dealing with large volumes of wastewater, batch processes are inadequate due to their discontinuous nature and inability to handle continuously generated effluents (Taka *et al*., 2020). Therefore, a more suitable approach involves utilizing MgFe-LDH as a fixed-bed column adsorbent. Fixed bed column adsorption is widely favoured in wastewater treatment due to its continuous operation, high efficiency, simplicity and economic feasibility, making it scalable from laboratory scale studies to industrial applications (Nuryadin and Imai, 2021a). Moreover, fixed bed columns facilitate the regeneration of MgFe-LDH through desorption processes, where, for instance, upto 73% of adsorbed phosphate can be effectively desorbed using a 0.1 M NaOH solution (Sun *et al*., 2013). This method allows for the recovery of phosphorus post regeneration, aligning with strategies to reclaim this non-renewable resource and preserve water quality. Chemical precipitation of phosphate into calcium phosphate emerges as an attractive option for phosphorus recovery from wastewater, given calcium phosphate's low solubility and potential use as an agricultural fertilizer (Nuryadin and Imai, 2021b). The feasibility of adsorbent regeneration and the subsequent application of regenerated by-products as fertilizers possibly enhance the cost effectiveness of using MgFe-LDH as an adsorbent.

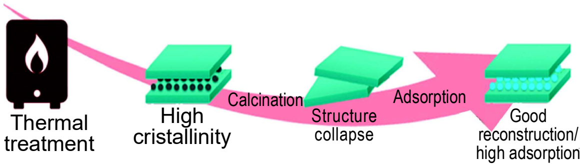

Fig. 8. Proposed illustration of the thermal aging effect on phosphate adsorption by MgFe-LDH.

Conclusion

The MgFe-LDH was successfully prepared and used for phosphate adsorption from water. In this study, thermally aged and calcined MgFe-LDH with an Mg to Fe ratio of 3 showed the maximum adsorption capacity. Pseudo-second-order kinetic modeling was the best model for predicting the observed phosphate adsorption behavior onto MgFe-LDH, showing that chemical interaction played a dominant role during the phosphate adsorption process. Intra-particle diffusion was not the only rate-limiting step in the adsorption process but consisted of two other processes, external surface diffusion and slow pore diffusion. According to XRD analysis, thermally aged MgFe-LDH had a high ability to adsorb phosphate due to its high crystallinity before calcination. The ability of calcined LDH to remove phosphate anions from an aqueous solution strongly depends on its structural re-construction. This indicates that a more ordered structure in the original uncalcined LDH enhances the removal of phosphate anions, resulting in a higher adsorption capacity in thermally aged calcined LDH compared to those aged at room temperature. This study offers additional insights to assist in synthesizing Mg-Fe-LDH for removing phosphate from water. Future work should investigate isotherm models e.g. (Langmuir, Freundlich, BET) to elucidate adsorption mechanisms and improve material performance.

Acknowledgement

The first author is delighted to acknowledge the support of the Indonesian Ministry of Research, Technology and Higher Education (RISTEK-DIKTI), as well as the Islamic Development Bank (IsDB) 4in1 Project Implementation Unit (PIU) for granting the scholarship.

Conflict of Interest. The authors declare that they have no conflict of interest.

References

Abdelkader, N.B.H., Bentouami, A., Derriche, Z., Bettahar, N., de Ménorval, L.-C. 2011. Synthesis and characterization of Mg-Fe layer double hydroxides and its application on adsorption of Orange G from aqueous solution. *Chemical Engine-*

ering Journal, **169:** 231-238.

Ahmed, A.A., Gypser, S., Leinweber, P., Freese, D., Kühn, O. 2019. Infrared spectroscopic characterization of phosphate binding at the goethite-water interface. *Physical Chemistry. Chemical Physics*, **21:** 4421-4434.

Akinpelu, A.A., Chowdhury, Z.Z., Shibly, S.M., Faisal, A.N.M., Badruddin, I.A., Rahman, M.M., Al Amin, M., Sagadevan, S., Akbarzadeh, O., Khan, T.M.Y., Kamangar, S., Khalid, K., Saidur, R., Johan, M.R. 2021. Adsorption studies of volatile organic compound (naphthalene) from aqueous effluents: chemical activation process using weak lewis acid, equilibrium kinetics and isotherm modelling. *International Journal of Molecular Sciences*, **22:** 2090.

Bacelo, H., Pintor, A.M.A., Santos, S.C.R., Boaventura, R.A.R., Botelho, C.M.S. 2020. Performance and prospects of different adsorbents for phosphorus uptake and recovery from water. *Chemical Engineering Journal*, **381:** 122566.

Bhavani, A.G., Wani, T.A., Ma'aruf, A., Prasad, T. 2021. Effect of ageing process on crystal morphology of Co-Mg-Al hydrotalcite. *Materials Today Proceeding*, **44:** 2277-2282.

Cavani, F., Trifirò, F., Vaccari, A. 1991. Hydrotalcite-type anionic clays: Preparation, properties and applications. *Catalysis Today*, **11:** 173-301.

Cosano, D., Esquivel, D., Romero-Salguero, F.J., Jiménez-Sanchidrián, C., Ruiz, J.R. 2020. Oleate epoxidation in a confined matrix of hydrotalcite. *American Chemical Society Omega*, **5:** 619-625.

Das, J., Patra, B.S., Baliarsingh, N., Parida, K.M. 2007. Calcined Mg-Fe-CO_3 LDH as an adsorbent for the removal of selenite. *Journal of Colloid and Interface Science*, **316:** 216-223.

Das, J., Patra, B.S., Baliarsingh, N., Parida, K.M. 2006. Adsorption of phosphate by layered double hydroxides in aqueous solutions. *Applied Clay Science*, **32:** 252-260.

Ding, Y., Dong, F., Zhao, J., Peng, W., Chen, Q., Ma, B. 2020. Non-point source pollution simulation and best management practices analysis based on control units in northern China. *International Journal of Environmental Research and Public Health*, **17:** 868.

Du, Y., Rees, N., O'Hare, D. 2009. A study of phosphate absorption by magnesium iron hydroxycarbonate. *Dalton Transactions*, **39:** 8197-8202.

Ferreira, O.P., Alves, O.L., Gouveia, D.X., Filho, A.G.S., de Paiva, J.A.C., Filho, J.M. 2004. Thermal decomposition and structural reconstruction effect on Mg-Fe-based hydrotalcite compounds. *Journal of Solid State Chemistry*, **177:** 3058-3069.

Goh, K.H., Lim, T.T., Dong, Z. 2008. Application of layered double hydroxides for removal of oxyanions: a review. *Water Research*, **42:** 1343-1368.

Hussein, M.Z.B., Taufiq-Yap, Y.H., Shahadan, R., Abd Rashid, N.Y. 2001. The effect of aging time on the properties of nickel-aluminium-carbonate layered double hydroxide synthesized by hydrothermal method. *Chemical Papers*, **55:** 273-278.

Iftekhar, S., Küçük, M.E., Srivastava, V., Repo, E., Sillanpää, M. 2018. Application of zinc-aluminium layered double hydroxides for adsorptive removal of phosphate and sulfate: equilibrium, kinetic and thermodynamic. *Chemosphere*, **209:** 470-479.

Kamimoto, Y., Okamoto, N., Hagio, T., Yong-Jun, J., Deevanhxay, P., Ichino, R. 2019. Development of magnesium-iron layered double hydroxide and application to nitrate removal. *Springer Nature Applied Sciences*, **1:** 1399.

Kim, T.-H., Lundehøj, L., Nielsen, U.G. 2020. An investigation of the phosphate removal mechanism by MgFe layered double hydroxides. *Applied Clay Science*, **189:** 105521.

Lai, Y.T., Huang, Y.S., Chen, C.H., Lin, Y.C., Jeng, H.T., Chang, M.C., Chen, L.J., Lee, C.Y., Hsu, P.C., Tai, N.H. 2020. Green treatment of phosphate from wastewater using a porous bio-templated graphene oxide/MgMn-layered double hydroxide composite. *iScience*, **23:** 101065.

Li, M., Liu, J., Xu, Y., Qian, G. 2016. Phosphate adsorption on metal oxides and metal hydroxides: a comparative review. *Environmental Reviews*, **24:** 319-332.

Liu, X., Zhang, L. 2015. Removal of phosphate anions using the modified chitosan beads: adsorption kinetic, isotherm and mechanism studies. *Powder Technology*, **277:** 112-119.

Liu, J., Zhou, Q., Chen, J., Zhang, L., Chang, N. 2013. Phosphate adsorption on hydroxyl-iron-lanthanum doped activated carbon fibre. *Chemical Engineering Journal*, **215-216:** 859-867.

Liu, W., Zhang, J., Zhang, C., Wang, Y., Li, Y. 2010. Adsorptive removal of Cr (VI) by Fe-modified activated carbon prepared from Trapa natans husk. *Chemical Engineering Journal*, **162:** 677-684.

Miyauchi, H., Yamamoto, T., Chitrakar, R., Makita, Y., Wang, Z., Kawai, J. Hirotsu, T. 2009. Phosphate adsorption site on zirconium ion modified MgAl-layered double hydroxides. *Topics in Catalysis*, **52:** 714-723.

Nguyen, D.-K., Dinh, V.-P., Dang, N.T., Khan, D.T., Hung, N.T., Tran, N.H.T. 2023. Effects of aging and hydrothermal treatment on the crystallization of ZSM-5 zeolite synthesis from bentonite. *Royal Society of Chemistry Advance*, **20:** 20565-20574.

Novillo, C., Guaya, D., Avendaño, A.A.P., Armijos, C., Cortina, J.L., Cota, I. 2014. Evaluation of phosphate removal capacity of Mg/Al layered double hydroxides from aqueous solutions. *Fuel*, **138:** 72-79.

Nuryadin, A., Imai, T. 2021a. Application of amorphous zirconium (hydr)oxide/MgFe layered double hydroxides composite in fixed-bed column for phosphate removal from water. *Global Journal of Environmental and Science Management*, **7:** 485-502.

Nuryadin, A., Imai, T. 2021b. Phosphorus desorption and recovery from aqueous solution using amorphous zirconium hydroxide/MgFe layered double hydroxides composite. *IOP Conference Series: Earth and Environmental Science*, **926:** 012107.

Nuryadin, A., Imai, T., Kanno, A., Yamamoto, K., Sekine, M., Higuchi, T. 2021. Phosphate adsorption and desorption on two-stage synthesized amorphous-ZrO_2/Mg-Fe layered double hydroxide composite. *Materials Chemistry and Physics*, **266:** 124559.

Osali, S., Ghiyasi, Y., Esfahani, H., Jose, R., Ramakrishna, S. 2023. Electrospun nanomembranes at the liquid-liquid and solid-liquid interface - a review. *Materials Today*, **67:** 151-177.

Peng, F., Luo, T., Yuan, Y. 2014. Controllable synthesis of Mg-Fe layered double hydroxide nanoplates with specific Mg/Fe ratios and their effect on adsorption of As(v) from water. *New Journal Chemistry*, **38:** 4427-4433.

Pholosi, A., Naidoo, E.B., Ofomaja, A.E. 2020. Intraparticle diffusion of Cr(VI) through biomass and magnetite coated biomass: a comparative kinetic and diffusion study. *South African Journal of Chemistry Engineering*, **32:** 39-55.

Qu, J. 2008. Research progress of novel adsorption processes in water purification: a review. *Journal of Environmental Sciences*, **20:** 1-13.

Raji, Z., Karim, A., Karam, A., Khalloufi, S. 2023. Adsorption of heavy metals: mechanisms, kinetics, and applications of various adsorbents in wastewater remediation - a review. *Waste*, **1:** 775-805.

Rápó, E., Tonk, S. 2021. Factors affecting synthetic dye adsorption, desorption studies: a review of results from the last five years (2017-2021). *Molecules*, **26:** 5419.

Sun, X., Imai, T., Sekine, M., Higuchi, T., Yamamoto, K., Akagi, K. 2013. Adsorption of phosphate by calcinated Mg-Fe layered double hydroxide. *Journal of Water and Environmental Technology*, **11:** 111-120.

Taka, A.L., Klink, M.J., Mbianda, X.Y., Naidoo, E.B. 2020. Chitosan nanocomposites for water treatment by fixed-bed continuous flow column adsorption: a review. *Carbohydrate Polymers*, **255:** 117398.

Tang, Z., Kong, N., Ouyang, J., Feng, C., Kim, N.Y., Ji, X., Wang, C., Farokhzad, O.C., Zhang, H., Tao, W. 2020. Phosphorus science-oriented design and synthesis of multifunctional nanomaterials for biomedical applications. *Matter*, **2:** 297-322.

Weber, W.J., Morris, J.C. 1963. Kinetics of adsorption on carbon from solution. *Journal of the Sanitary Engineering Division*, **89:** 31-59.